Scientific Visualization, 2023, volume 15, number 1, pages 47 - 59, DOI: 10.26583/sv.15.1.04

Modeling and Visualization of Electron Scattering on Quantum Rings

E.A. Muzykina[1], Y.D. Sibirmovsky[2]

National Research Nuclear University MEPhI (Moscow Engineering Physics Institute), Moscow, Russia

[1] ORCID: 0000-0001-8712-3625, kotya.muzykina@mail.ru
[2] ORCID: 0000-0001-5101-3336, YDSibirmovsky@mephi.ru

Abstract

The problem of scattering of two-dimensional electrons on a potential in the form of a quantum ring and a quantum dot is solved. The problem is addressed as a part of analysis of quantum interference effects in semiconductor nanostructures with nontrivial geometry as well as for the design of nanoelectronic devices based on them. In contrast to existing works, algorithms for solving both stationary and non-stationary Schrödinger equation with arbitrary scattering potential are developed here. Analytical and finite-difference methods are used, which makes it possible to obtain an arbitrarily accurate solution, with which the process of electron scattering on a quantum ring is modeled and visualized. This visualization allows us to discover how the shape of the quantum ring affects the angular distribution of the scattering amplitude as well as determine the presence of a self-interference of the scattered electron wave function.

Keywords: quantum scattering, quantum rings, quantum dots, wave packet.

1 Introduction

Hybrid systems consisting of a semiconductor quantum well and a layer of quantum dots or rings are studied as a part of materials design for electronics and photonics devices, due to their photoconductive properties and unique magnetoresistance and carrier transport properties [1-7]. The examples are, the change of conductivity under illumination, the negative refractive index for certain wavelengths, oscillations of magnetoresistance. Such systems also exhibit topological properties that can be controlled by electric and magnetic fields - the Aharonov-Bohm effect and other quantum interference effects arising from scattering of electrons on an array of quantum structures in a magnetic field.

The simulation presented in this work is also carried out for explanation of the results of the experimental paper [1], which investigates the electronic and optical properties of hybrid systems with quantum rings (Figure 1). The scattering of electrons on quantum rings and quantum dots of different shapes is simulated and visualized. The two-dimensional Schrödinger equation for the stationary and non-stationary problem is solved by different methods. The square of the modulus of the wave function is constructed for several potential forms, and the reduced 2D scattering cross section and the probability current are calculated. To perform the calculations and visualize the results (such as wave functions and probability currents) original programs were written by the authors, using R and Rust programming languages.

Some of the existing scientific works experimentally investigate the properties of arrays of quantum rings and dots. The second group of papers studies mainly the calculation of the optical properties of quantum rings when electrons scatter on them in a transverse magnetic field [6-8]. Some papers investigate the motion along a channel that splits at a certain point to form a ring [9, 10].

The [9] demonstrates the solution of the scattering problem using the finite-difference method. The potential was represented in the form of a locally partitioned channel; the main task was to investigate two variants of open boundary conditions.

The work [10] investigates the wave packet scattering. The ring-like channels of various shapes were used: circular, rectangular, semicircular. There was also an additional channel connecting the ring at two more points. The main task was to study the dependence of the wave packet dynamics on the width of the additional channel.

There are also papers investigating two-dimensional scattering on a rigid disk [11] or solving the problem of scattering and searching for energy levels [12, 13].

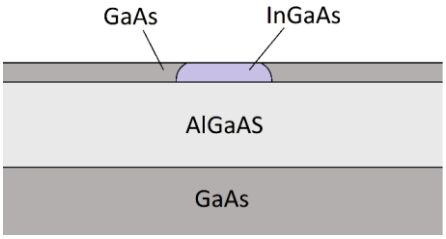

Figure 1 – Example of a hybrid system consisting of a quantum well and a quantum dot.

2 Problem statement and methods

In this paper we study hybrid systems consisting of a semiconductor quantum well and a layer of quantum rings or quantum dots. Quantum rings and dots are zero-dimensional structures, quantum well is two-dimensional. This means that for the scattering problem it is necessary to solve the Schrödinger equation.

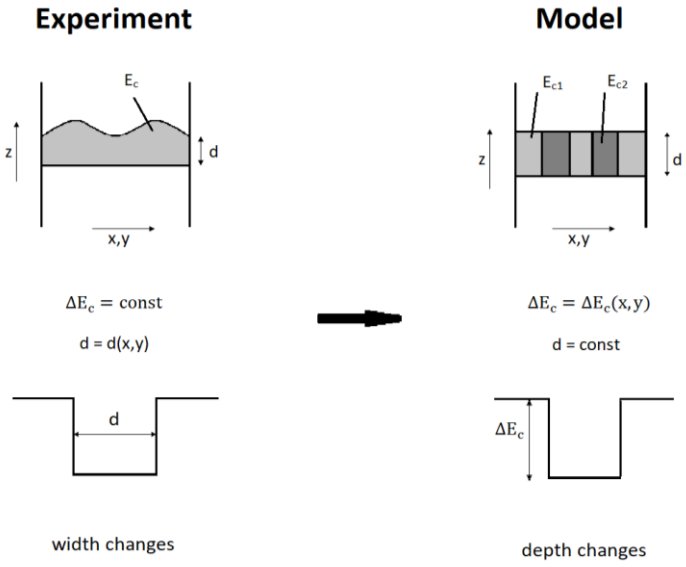

Figure 2 – Comparison of computational model and experimental structure.

In the usual experimental set up the quantum ring represents a local expansion of the potential well, i.e. it is necessary to consider the three-dimensional motion of particles, which is quite difficult to model [1,5]. In our computational model, the change in the depth of the well is considered, while the width remains constant, which allows us to solve the two-dimensional problem. A visual comparison of the two approaches is presented in Figure 2. The model is qualitatively consistent with the experiment. Calculation of two-dimensional scattering is much easier than three-dimensional scattering, and thanks to this approach it is possible to consider many different configurations.

The main purpose of this work is to solve and simulate the problem of scattering of electron flux on a potential in 2D. Two different formulations of this problem are considered. Stationary (1) and time-dependent one (2), where $\widehat{H}$ is the Hamiltonian operator.

$$\widehat{H} = -\frac{\hbar^2}{2m}\Delta + U$$

$$\begin{cases} \widehat{H}\psi(r,\theta) = E\psi(r,\theta), \quad 0 < r < \infty, -\pi < \theta < \pi \\ |\psi(0,\theta)| < \infty \\ \psi(r \to \infty, \theta) = e^{ikr\cos\theta} + f(\theta)\dfrac{e^{ikr}}{\sqrt{kr}}e^{i\frac{\pi}{4}} \end{cases} \tag{1}$$

where $\hbar$ is Planck's constant, m the effective mass of the electron in the quantum well material, i is imaginary unit, Δ is the Laplace operator, (r,θ) are the polar coordinates: radius and polar angle, $\psi(r,\theta)$ is the wave function, $U(r,\theta)$ is the potential function, E is the electron energy, $f(\theta)$ is the scattering amplitude. The phase multiplier $e^{i\frac{\pi}{4}}$ is necessary to agree with the optical theorem [11].

$$\begin{cases} i\hbar\dfrac{\partial}{\partial t}\psi(t,x,y) = \widehat{H}\psi(t,x,y) \\ 0 \le x \le L_x, |y| \le L_y \\ \psi(0,x,y) = \xi(x,y) \\ \psi(t,0,y) = \psi(t,L_x,y) = \psi\big(t,x,L_y\big) = \psi\big(t,x,-L_y\big) = 0 \end{cases} \tag{2}$$

where t – time, $\frac{\partial}{\partial t}$ is the time partial derivative, (x,y) is the Cartesian coordinates, $\xi(x,y)$ is the initial function whose form and meaning we will consider later, L_x, L_y are the boundaries of the computational domain.

The probability current along the x-axis was calculated using formula (3). The electric current density depends on the probability current density, namely: $\overrightarrow{J_e} = e\vec{J}$, where $\overrightarrow{J_e}$ is the electric current density.

$$J_x = \frac{\hbar}{2mi}\left(\psi^*\frac{\partial\psi}{\partial x} - \psi\frac{\partial\psi^*}{\partial x}\right) \tag{3}$$

To solve the stationary problem, at first Born approximation had been considered; in the articles found, it was used mainly to solve the inverse scattering problems.

However this method is not suitable in the present case because of the values of the parameters for which the calculation was carried out (Table 1) - the condition of small potential is not satisfied: $|U| \le \frac{\hbar^2}{mL}$.

2.1 Fourier Method

The second method for solving the stationary problem is based on expanding the desired wave function into a Fourier series (4), that defines the methods name. Substituting the series into the Schrödinger equation, we obtain the equation for the expansion coefficients. Boundary conditions (5) are also expanded (6).

$$\psi(r,\theta) = \frac{1}{\sqrt{2\pi}}\sum_{l_\theta=-N_\theta}^{N_\theta} C_{l_\theta}(r)\, exp\,(il_\theta\theta) \tag{4}$$

$$\psi(r \to \infty, \theta) = e^{ikrcos\,\theta} + f(\theta)\frac{e^{ikr}}{\sqrt{r}}e^{\frac{i\pi}{4}} \tag{5}$$

$$C_{j_\theta}(r \to \infty) = i^{|j_\theta|}J_{|j_\theta|}(kr) + F_{j\theta}\frac{e^{ikr}}{\sqrt{kr}}e^{\frac{i\pi}{4}} \tag{6}$$

$$f(\theta) = \frac{1}{\sqrt{2\pi}} \sum_{j_\theta=-N_\theta}^{N_\theta} F_{j\theta}\ exp\ (ij_\theta\theta)$$

In this paper we consider the solution of the equation for local axially symmetric potentials, which can be approximately partitioned into constant-value steps (7). The proposed method can be used for potentials with no symmetry as well, but it would require to solve a large system of equations.

$$U(r) = \begin{cases} U_1, & 0 \le r \le r_1 \\ U_2, & r_1 \le r \le r_2 \\ \dots & \\ U_i, & r_{i-1} \le r \le r_i \\ \dots & \\ 0, & r_{N-1} \le r_N \end{cases} \tag{7}$$

For one constant value of the potential U_0 we obtain equation (8). The solution of this equation is a linear combination of Bessel functions of the first and second kind (9).

$$-\frac{1}{r}\frac{d}{dr}\left(r\frac{dC_{j_\theta}}{dr}\right) + \left[\frac{1}{r^2}j_\theta^2 - (k^2 - u_0)\right]C_{j_\theta} = 0 \tag{8}$$

$$u_0 = \frac{2m}{\hbar^2}U_0$$

$$C_{j\theta}(r) = P\,J_{j\theta}\left(\sqrt{k^2 - u_0}r\right) + Q\,Y_{j\theta}\left(\sqrt{k^2 - u_0}r\right) \tag{9}$$

For the first region $0 \le r \le r_1$ the solution always contains only the Bessel function of the first kind since the solution must be finite at zero.

2.2 Finite-difference method

The finite-difference method has been developed to solve the time-dependent problem. The electron is replaced by the wave packet (10), where x_0 is the initial position, a is the initial dispersion. These are the additional free parameters, compared to the stationary case.

$$\xi(x,y) = \frac{1}{\sqrt{\sqrt{2\pi}a}}\frac{1}{\sqrt{L_y}}e^{ik(x-x_0)-\frac{(x-x_0)^2}{2a^2}}\sin\left[\frac{\pi}{2}\left(1-\frac{y}{L_y}\right)\right] \tag{10}$$

$$i\hbar\frac{\partial}{\partial t}\psi(t,x,y) = \left(-\frac{\hbar^2}{2m}\Delta + U(x,y)\right)\psi(x,y)$$

$$\tau = \frac{\hbar}{2m}t$$

There is a grid with variables x, y .

$$x \in [0, L_x], j_x = 1, \dots, N_x$$

$$y \in [-L_y, L_y], j_y = -N_y, \dots, N_y$$

The coordinate derivatives are replaced by the finite-difference approximation according to the equation (11), where $\psi_{j_x j_y}$ is the value of the wave function on the coordinate grid. The probability current was calculated according to the formula (12), which is a finite-difference representation of (3).

$$i\frac{\partial}{\partial\tau}\psi_{j_x j_y} = -\frac{\psi_{j_x-1 j_y} - 2\psi_{j_x j_y} + \psi_{j_x+1 j_y}}{\Delta x^2} - \frac{\psi_{j_x j_y-1} - 2\psi_{j_x j_y} + \psi_{j_x j_y+1}}{\Delta y^2} + u_0(x_{j_x}, y_{j_y})\psi_{j_x j_y} \tag{11}$$

$$J_{x\,j_x j_y} = \frac{i\hbar}{4m\Delta x}\left(\psi^*_{j_x j_y}\left(\psi_{j_x+1 j_y} - \psi_{j_x-1 j_y}\right) - \psi_{j_x j_y}\left(\psi^*_{j_x+1 j_y} - \psi^*_{j_x-1 j_y}\right)\right) \tag{12}$$

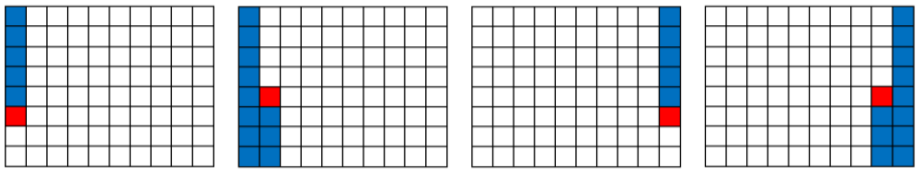

Figure 3 – Scheme of bypassing all grid points.

The finite-difference time scheme is based on the asymmetric Sauliev scheme [14], which on the one hand is explicit, which simplifies the algorithm, and on the other hand is more stable and leads to less error than other explicit schemes. This scheme can be proven to be unconditionally stable, but in its asymmetric form (moving along the grid in one direction) doesn't preserve the norm of the wave function. Switching directions at each step as it's done here greatly improves the norm stability.

A full description of the finite-difference scheme is given in Appendix 1.

3 Simulation results and discussion

Table 1 shows the values of the parameters for which the calculations were carried out. In this work several models of quantum rings and dots were investigated, 3D image and section of which are shown in Figure 4 (U_0 – characteristic value of the potential).

The parameter values correspond to the experimental samples from the article [1]. In this study, a quantum well of 6 nm width was investigated, and the distance between the bottom of the first subband and the top of the quantum well was 0.08 eV.

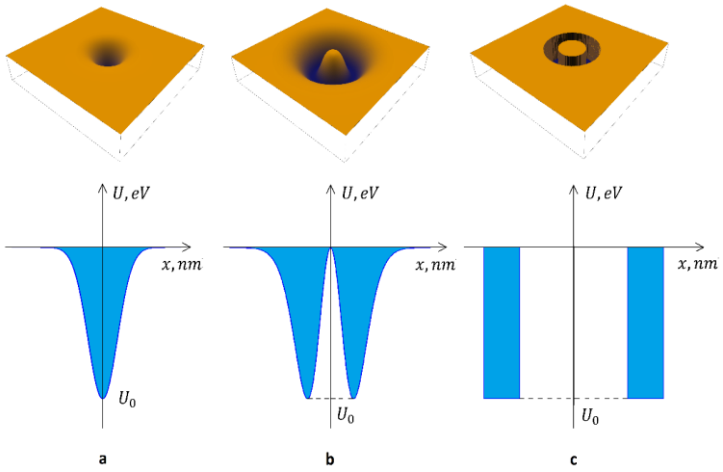

Figure 4 – Examples of investigated potential holes: a) as a Gaussian function, b) the difference of two Gaussian functions, c) as a cylindrical ring.

Table 1. Values of the parameters for which the calculation was carried out.

Quantum well width d, nm	6
Effective mass of the electron, m (m_0 is the mass of the electron in a vacuum)	$m = 0.067\ m_0$
Distance between the bottom of the first subzone and the top of the quantum well ΔE, eV	0.08
Electron energy E, eV	0.01 ÷ 0.1
The depth of the potential pit U_0, eV	-0.2
Outer ring radius R_1, nm	30 ÷ 100
Inner radius of the ring R_2, nm	(0.3 ÷ 0.7) R_1

3.1 Fourier method

To solve the scattering problem with this method, it is necessary to divide the potential into a set of steps with a constant value (equation (7)). For a cylindrical ring we get 3 sections with a constant value of the potential. For the potentials in the form of Gaussian functions significantly more steps is required. An example of potential partitioning for a ring is shown in Figure 5. Along the radius-vector axis, the value of the function on the left boundary is taken at equal intervals. The potential is equated to zero, when the value of the Gaussian function is less than $1 \cdot 10^{-12}$.

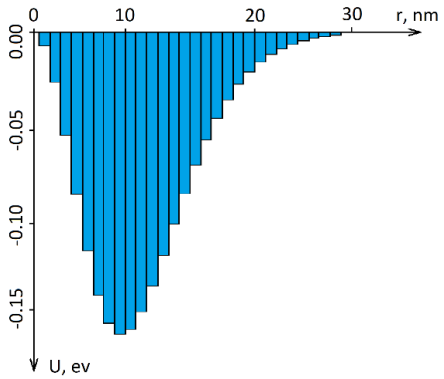

Figure 5 – Gaussian potential divided into columns with the same value.

The calculation has been carried out for different energy values. Plots of the probability current dependence on energy for different potentials are shown in Figure 6. For rings a plateau after a certain value of energy is noticeable, for the cylindrical form it appears earlier. For a quantum dot a smooth increase in the probability current is observed. The obtained dependences qualitatively correspond to the behavior of the probability current in the case of quantum tunneling.

Figures 7 and 8 show a comparison of the squared modulus of wave functions and the reduced 2D scattering cross section for reduced potentials for an energy of 0.5 eV. It can be seen that the cylindrical potential well is characterized by multiple centers of oscillations. This is due to additional reflections from the ring boundaries. For the Gaussian potentials this is not observed, which is due to the smoothness and continuity of the function.

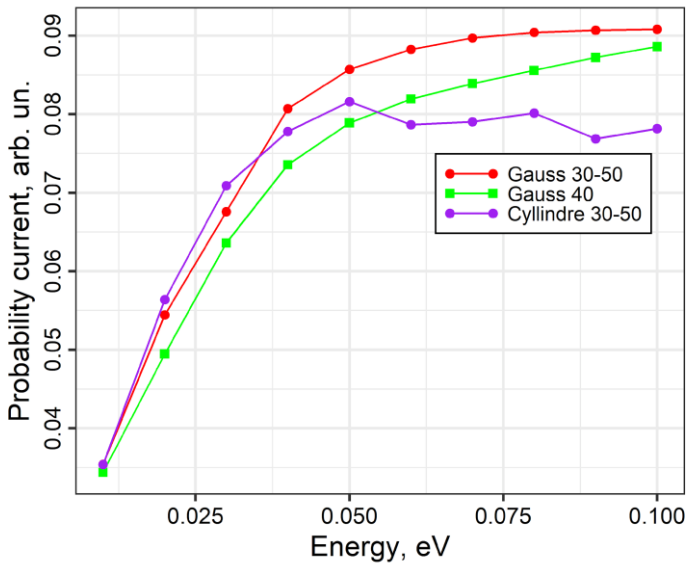

Figure 6 – Plot of probability current versus energy for different potentials: red line - Gaussian ring with radii of 30 and 50 nm; green - Gaussian quantum dot with radius of 40 nm;

purple - cylindrical ring with radii of 30 and 50 nm.

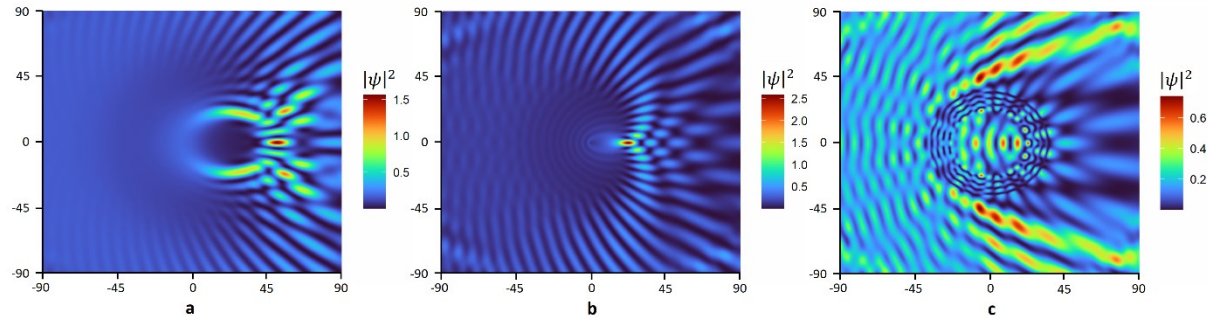

Figure 7 – Square of the wave function modulus for potentials: a - Gaussian ring with radii of 30 and 50 nm; b - Gaussian point with radius of 40 nm;
c - cylindrical ring with radii of 30 and 50 nm.

When comparing the scattering patterns, one can see that for a Gaussian ring there is a movement through both parts of the ring, followed by interference (Figure 7(a)). For a quantum dot, the wave function is focused at the center of the nanostructure (Figure 7(b)).

When comparing the scattering cross section, forward scattering mainly occurs for all three cases. For the Gaussian ring, additional maxima located close to zero. This corresponds to the interference of the parts of the wave function coming out of the potential well (Figure 8(a)). For a cylindrical ring we see smaller maxima at some distance from zero (Figure 8(c)), they correspond to the parts of the wave function that did not fall into the well. For the quantum dot the central maximum is greater in intensity than for the rings, and there are also small additional maxima (Figure 8(b)).

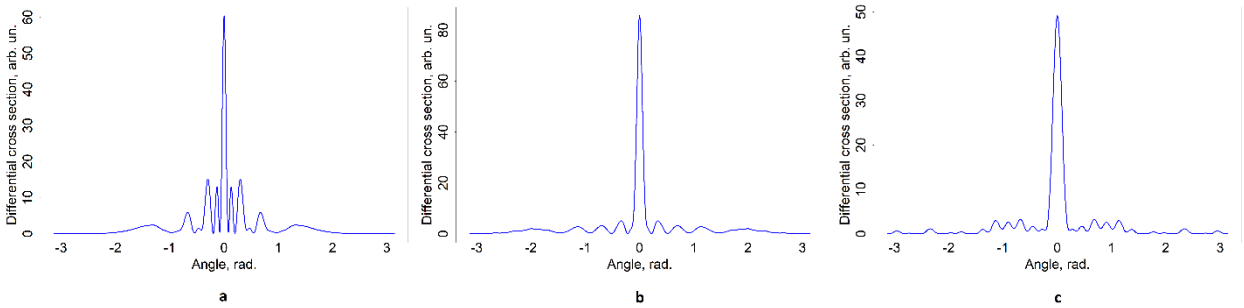

Figure 8 – The reduced 2D scattering cross section for the potentials: a - Gaussian ring with radii of 30 and 50 nm; b - Gaussian point with radius of 40 nm;
c - cylindrical ring with radii of 30 and 50 nm.

The problem of scattering on a disk-shaped barrier was solved in the paper [11]. The Fourier method given above is also suitable for such a problem, which allows us to compare the results. Qualitatively and numerically the solutions coincide, the squares of the modulus of wave functions and the reduced 2D scattering cross sections were compared: $\sigma = k|f(\theta)|^2$.

The program with the implementation of this method is written in R, the system of linear equations for the expansion coefficients is solved using the built-in function solve(). The visualization of the square of the modulus of the wave function is done using the ggplot2 library: an image is created from the given array with the values of the function.

3.2 Finite-difference method

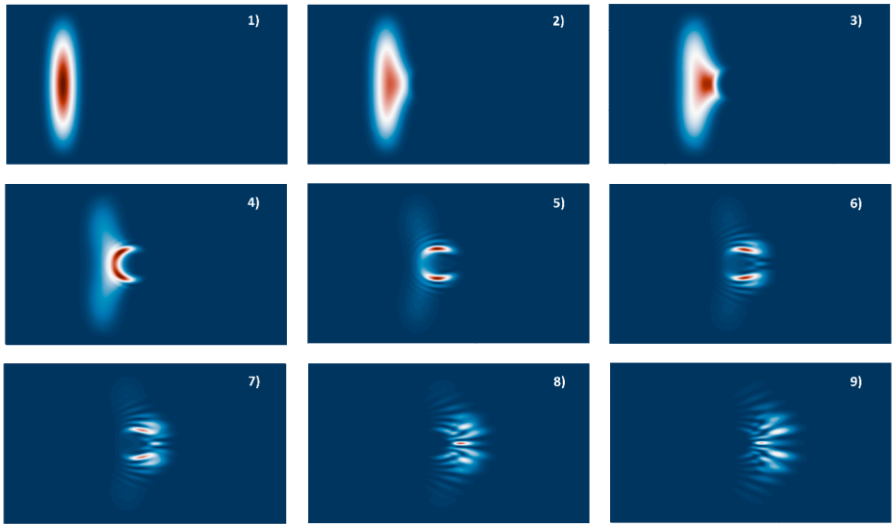

Figure 9 – The motion of the wave packet (the square of the wave function modulus) during scattering on a Gaussian quantum ring.

The finite-difference method was developed for a time-dependent problem. Examples of the results of the scattering problem are presented in Figures 9-11 for the cylindrical and Gaussian quantum ring, Gaussian quantum dot, respectively. It can be seen that for the quantum ring the wave packet is divided into two identical parts, while for the quantum dot the scattering is focused inside the nanostructure.

The program for this method is written in the Rust programming language. As a result, we obtain images of the potential and position of the wave packet at several points in time. To visualize the motion of the wave packet, a custom function was implemented that translates the values of the square of the modulus of the wave function on the grid into integers from 0 to 99 with known maximum and minimum values. They are correlated with color values from a given palette of 100 colors.

In Figures 9-11 the size of the calculation area is 500 nm (the x axis) by 300 nm (the y axis).

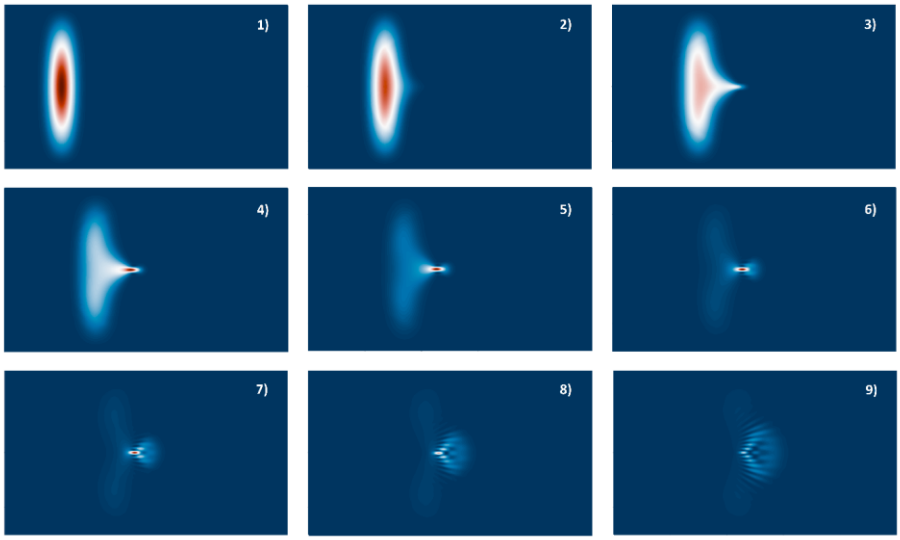

Figure 10 – The motion of the wave packet (square of the modulus of the wave function) at scattering on a Gaussian quantum dot.

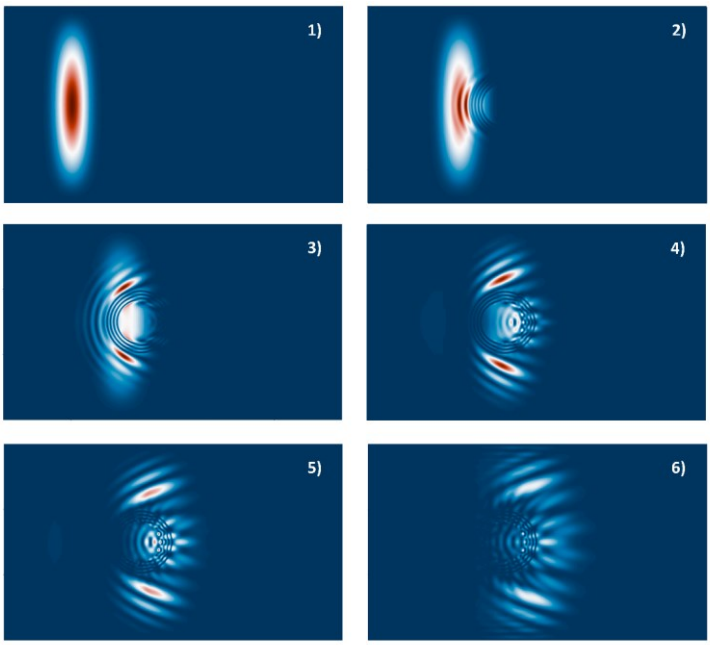

Figure 11 – Motion of the wave packet (square of the wave function modulus) when scattering on a hole in the form of a ring with radii of 30 and 50 nm.

A comparison of the results obtained by the Fourier method and the finite-difference method is shown in Figure 12. The pictures are similar: the main centers of oscillations and the position of parts of the wave packet, their shape and direction coincide. The finite-difference method produces a sequence of images with a scattering picture with some time step. Because of this the states may not coincide.

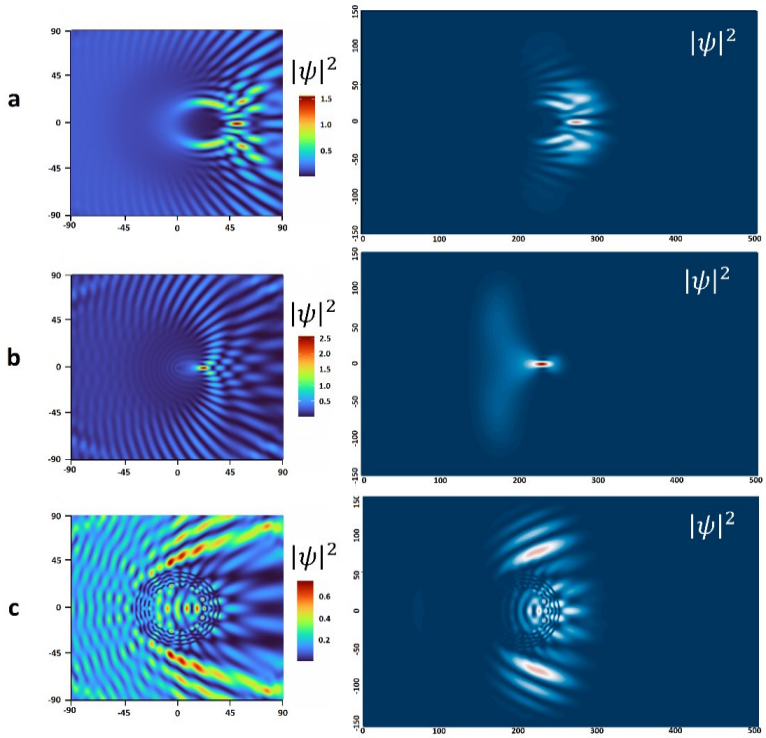

Figure 12 – Comparison of the Fourier method (left) and the finite-difference method (right): a - for a Gaussian ring; b - for a Gaussian point; c - for a cylindrical ring.

4 Conclusions

The Fourier method and the finite-difference method both cope very well with solving the problem of two-dimensional electron scattering on the considered potentials. Visualization of the wave function and probability current confirms the correctness of the developed programs by comparing the visualized results with other existing works and with each other. The obtained images of the quantities sought show that the results of both methods are physically meaningful and consistent with each other.

The results of the Fourier method for another problem were compared to the article [11] and found to be in agreement. A solution for centrally symmetric potentials has been developed. But the method is not limited to this condition. For an arbitrary form of potential, it is necessary to solve a large system of equations. The only requirement for using this method is to divide the potential into several piecewise constants.

The developed finite-difference method is suitable for any shapes and positions of the potential. To solve the problem, it is necessary to specify its values on the coordinate grid. For the developed method, the most important thing is the ratio of intervals between neighboring grid points for the three variables. Even though the Sauliev scheme for the Schrödinger equation can be proven to be unconditionally stable, in practice a sufficiently small time interval is required for the computational scheme to converge.

When using wave packets to model scattering, one needs to consider the widening of the wave packet as it moves. The speed of the widening is inversely proportional to the initial width. Thus, two free parameters appear - the initial position of the wave packet and the initial width (dispersion), which require careful selection.

The obtained solutions demonstrate that scattering on a quantum ring devides the wave function into two equal parts. For the quantum dot we see the focusing of the wave function inside the nanostructure.

Acknowledgements

The present work was supported by the Ministry of Science and Higher Education within the framework of the Russian State Assignment under contract No FSWU-2023-0075.

References

[1] Y D Sibirmovsky, I S Vasil'evskii, A N Vinichenko, D M Zhigunov, I S Eremin, O S Kolentsova, D A Safonov, N I Kargin, Electronic and optical properties of HEMT heterostructures with δ-Si doped GaAs/AlGaAs quantum rings – quantum well system, Journal of Physics: Conf. Series 917 (2017), doi: 10.1088/1742-6596/917/3/032041.

[2] Masafumi Jo, Takaaki Mano, Kazuaki Sakoda, Morphological control of GaAs quantum dots grown by droplet epitaxy using a thin AlGaAs capping layer, Journal of applied physics 108, (2010), doi: 10.1063/1.3493262.

[3] Min Song, Jiun-haw-Chu, Jian Zhou, Sefaattin Tongay, Kai Liu, Joonki Suh, Henry Chen, Jeong Seuk Kang, Xuecheng Zou, Long You, Magnetoresistance oscillations in topological insulator Bi_2Te_3 nanoscale antidot arrays, Nanotechnology 26 (2015), doi: 10.1088/0957-4484/26/26/265301

[4] Vladimir M. Fomin, "Quantum ring: a unique playground for the Quantum-Mechanical Paradigm", Physics of Quantum Rings Chapter 1, 2018, pp. 3-32, doi: 10.1007/978-3-319-95159-1_1.

[5] Y. D. Sibirmovsky, Mechanismy formirovania, opticheskie i electronnye transportnye svoystva ansamblya quantovyh kolec GaAs/AlGaAs, PhD thesis, Moscow, 2018. – 139 p.

[6] Xiaojing Li, Magnetoexciton in semiconductor concentric double rings, Physica E 41 (2009), doi: 10.1016/j.physe.2009.07.005.

[7] F.J. Culchac, N. Porras-Montenegro, A. Latge, GaAs-(Ga,Al)As double quantum rings: confinement and magnetic field effect, J. Phys.: Condens. Matter 20 (2008), doi: 10.1088/0953-8984/20/28/285215.

[8] M. Grohol, F. Grosse, R. Zimmermann, "Optical exciton Aharonov-Bohm effect, persistent current, and magnetization in semiconductor nanorings of type I and II", Physical Review B 74, (2006), doi: 10.1103/PhysRevB.74.115416.

[9] J.-F. Mennemann, A. Jüngel, Perfectly Matched Layers versus discrete transparent boundary conditions in quantum device simulation, Journal of Computational Physics 275 (2014). 1-24, doi: 10.1016/j.jcp.2014.06.049.

[10] Ariel Adorno Sousa A Sousa, A. Chaves, T.A.S. Pereira, G. de A. Farias, F.M. Peeters Peeters, Wave packet propagation through branched quantum rings under applied magnetic field, Physica E: Low-dimensional Systems and Nanostructiures 114 (2019), doi: 10.1016/j.physe.2019.113598.

[11] S. McAlinden, J. Shertzer, Quantum scattering from cylindrical barriers, American Journal of Physics 84, 764 (2016), doi: 10.1119/1.4960021.

[12] A. A. Bryzgalov, F. I. Karmanov, Method for splitting into physical processes in the problem on the time dynamics of electron wave functions of a two-dimensional quantum ring, Mathematical Models and Computer Simulations volume 3, 25–34 (2011), doi: 10.1134/S2070048211010029.

[13] E. V. Antropova, A. A. Bryzgalov, F. I. Karmanov, Urovni energii i sobstvenye volnovye functii electronov system quantovyh kolec v magnitnom pole, Vestn. Sam. gos. techn. un-ta. Ser. Phys.-mat. nauki, 2013, issue 1(30), pp. 326-333, doi: 10.14498/vsgtu1171.

[14] Sauliev V.K. Integrirovanie uravneniy parabolicheskogo tipa metodom setok, Physmatgiz, 1960. - 324 p.

Appendix

To solve the non-stationary problem, the time grid is also introduced:

$$\tau \in [0, T], n = 0, \dots, N_t$$

$$\Delta\tau = \frac{T}{2N_t + 2}$$

As indicated in Figure 3 in the computational scheme, the motion goes in four directions. The equation for the wave function of each grid point for each direction is (A.1-A.4), where the index on top denotes the time step, $u_{j_x j_y}$ is the potential value on the coordinate grid. The time derivative and the value of the wave function at the required point of the grid are written out according to the Sauliev finite-difference scheme [14].

$$\begin{aligned} i\frac{\psi^{(2n+1)}_{(2j_x-1)j_y} - \psi^{(2n)}_{(2j_x-1)j_y}}{\Delta\tau} &= -\frac{\psi^{(2n+1)}_{(2j_x-2)j_y} - \psi^{(2n+1)}_{(2j_x-1)j_y} - \psi^{(2n)}_{(2j_x-1)j_y} + \psi^{(2n)}_{(2j_x)j_y}}{\Delta x^2} \\ &- \frac{\psi^{(2n)}_{(2j_x-1)j_y-1} - \psi^{(2n)}_{(2j_x-1)j_y} - \psi^{(2n+1)}_{(2j_x-1)j_y} + \psi^{(2n+1)}_{(2j_x-1)j_y+1}}{\Delta y^2} \\ &+ \frac{1}{2}u_{(2j_x-1)j_y}\left(\psi^{(2n+1)}_{(2j_x-1)j_y} + \psi^{(2n)}_{(2j_x-1)j_y}\right) \end{aligned} \tag{A.1}$$

$$
\begin{aligned}
& i\frac{\psi_{(2j_x)j_y}^{(2n+1)}-\psi_{(2j_x)j_y}^{(2n)}}{\Delta\tau} \\
&= -\frac{\psi_{(2j_x-1)j_y}^{(2n+1)}-\psi_{(2j_x)j_y}^{(2n+1)}-\psi_{(2j_x)j_y}^{(2n)}+\psi_{(2j_x+1)j_y}^{(2n)}}{\Delta x^2} \\
&\quad -\frac{\psi_{(2j_x)j_y-1}^{(2n+1)}-\psi_{(2j_x)j_y}^{(2n+1)}-\psi_{(2j_x)j_y}^{(2n)}+\psi_{(2j_x)j_y+1}^{(2n)}}{\Delta y^2} \\
&\quad +\frac{1}{2}u_{(2j_x)j_y}\left(\psi_{(2j_x)j_y}^{(2n+1)}+\psi_{(2j_x)j_y}^{(2n)}\right)
\end{aligned}
\tag{A.2}
$$

$$
\begin{aligned}
& i\frac{\psi_{(2j_x)j_y}^{(2n+2)}-\psi_{(2j_x)j_y}^{(2n+1)}}{\Delta\tau} \\
&= -\frac{\psi_{(2j_x-1)j_y}^{(2n+1)}-\psi_{(2j_x)j_y}^{(2n+1)}-\psi_{(2j_x)j_y}^{(2n+2)}+\psi_{(2j_x+1)j_y}^{(2n+2)}}{\Delta x^2} \\
&\quad -\frac{\psi_{(2j_x)j_y-1}^{(2n+1)}-\psi_{(2j_x)j_y}^{(2n+1)}-\psi_{(2j_x)j_y}^{(2n+2)}+\psi_{(2j_x)j_y+1}^{(2n+2)}}{\Delta y^2} \\
&\quad +\frac{1}{2}u_{(2j_x)j_y}\left(\psi_{(2j_x)j_y}^{(2n+2)}+\psi_{(2j_x)j_y}^{(2n+1)}\right)
\end{aligned}
\tag{A.3}
$$

$$
\begin{aligned}
& i\frac{\psi_{(2j_x-1)j_y}^{(2n+2)}-\psi_{(2j_x-1)j_y}^{(2n+1)}}{\Delta\tau} \\
&= -\frac{\psi_{(2j_x-2)j_y}^{(2n+1)}-\psi_{(2j_x-1)j_y}^{(2n+1)}-\psi_{(2j_x-1)j_y}^{(2n+2)}+\psi_{(2j_x)j_y}^{(2n+2)}}{\Delta x^2} \\
&\quad -\frac{\psi_{(2j_x-1)j_y-1}^{(2n+2)}-\psi_{(2j_x-1)j_y}^{(2n+2)}-\psi_{(2j_x-1)j_y}^{(2n+1)}+\psi_{(2j_x-1)j_y+1}^{(2n+1)}}{\Delta y^2} \\
&\quad +\frac{1}{2}u_{(2j_x-1)j_y}\left(\psi_{(2j_x-1)j_y}^{(2n+2)}+\psi_{(2j_x-1)j_y}^{(2n+1)}\right)
\end{aligned}
\tag{A.4}
$$